31st Annual International Conference of the IEEE EMBS
Minneapolis, Minnesota, USA, September 2-6, 2009

A 2D Post-beamforming Filter for Contrast Restoration in Medical Ultrasound: *In Vivo* Results

Yayun Wan and Emad S. Ebbini

Abstract— **We have recently developed a robust 2D post-beamforming filter for contrast restoration in ultrasound imaging systems using coarsely-sampled array apertures, e.g. high frequency ultrasound (HFUS). The filter can be derived from a discretized 2D impulse response model in the region of interest (ROI). The key to the robustness of the regularized 2D pseudoinverse filter is transforming the operator to k-space, where the regularized inversion is implemented using 2D DFT instead of computationally intractable matrix operations. Using computer simulations, the 2D PIO was shown to produce complete restoration of contrast loss due to grating lobes resulting from coarse, 2λ sampling of HFUS arrays in the 25 - 35 MHz range. In this paper, we present the first *in vivo* demonstration of the 2D PIO in imaging the carotid artery using a commercially available probe. The results show that the 2D PIO increases the tissue/blood contrast by 4 dB (when imaging a cross section of the vessel). These results are in agreement with experimental results obtained using the same probe in imaging quality assurance phantoms. The 2D PIO's ability to remove the clutter from grating lobe is expected to improve the performance of speckle tracking algorithms for the estimation of tissue and blood displacements *in vivo*.**

I. INTRODUCTION

High-frequency ultrasound (HFUS) ($\geq$ 20 MHz) has emerged as an important tool for noninvasive visualization of living tissues at or near microscopic levels in many clinical or biological applications, such as dermatology [1], ophthalmology [2], [3], intravascular & intracardiac imaging [4]–[6], nonvascular endoluminal imaging [7], cartilage imaging [8], and especially small-animal studies [9]. High-frequency systems with single-element transducers has been commercialized for several years while the ones with (linear) array transducers just released recently [10], [11].

Great efforts have been put into the fabrication of array transducers for HFUS imaging applications [12]–[19]. These investigation are motivated by the success of array transducers in clinical applications in the frequency range of 2 - 16 MHz. A typical linear array in this frequency range is implemented with element-to-element spacing in the 1 - 1.2 λ range with minimal grating lobe artifacts. Due to the small element size requirement for high frequency arrays, it is expected that there is increased difficulty on array fabrication, such as increased cross coupling, increased element impedance, and increased variability in element sensitivity. Therefore, the majority of HFUS linear arrays in the range of 20 - 60 MHz are realized with 1.5 - 3 λ pitch (rather than the desirable range of 1 - 1.2 λ for linear array imaging) [10], [15], [16]. Conventional beamforming with these coarsely sampled arrays results in increased grating lobe levels leading to reduced dynamic range and loss of contrast.

We have proposed a post-beamforming 2-dimensional (2D) pseudoinverse filtering algorithm: 2D PIO filter for restoring the loss of contrast due to beamforming artifacts using coarsely sampled arrays [20]. Pseudoinverse and matched filtering has been successfully used in ultrasonic imaging to restore axial resolution, primarily in conjunction with coded excitation [21]–[25]. The pseudoinverse filtering algorithm in [21], [26] employs a filter bank for parallel processing of echo data from multiple directions from a single beamforming operation. In the 2D PIO filtering algorithm [20], the single-line model is extended to include data from multiple A-lines (up to a frame) by axial and lateral shifting of the 2D impulse response of the single-line beamforming operation, leading to a 2D (spatial and temporal) operator for reconstruction. Generally, the imaging process of retrieving the scatterer distribution from the received echo requires the inversion of the propagation matrix. A direct inversion of the propagation matrix is theoretically possible but requires excessive memory (typically above 100 GB) and number of operations. Our approach takes advantage of the propagation matrix structure and circulant-block block circulant (CBBC) matrices approximations [20], transforming infeasible inversion operations to computationally-efficient FFT operations. The 2D PIO filtering algorithm not only improves the computational efficiency and reduces the storage cost, but also transforms a usually ill-posed inverse problem to a well-posed FFT problem. Therefore, the 2D PIO filtering approach offers the promise of realizing the benefits of high-resolution ultrasonic imaging using coarsely sampled apertures.

Simulation and experiments on quality-assurance phantoms have been presented for verifying the performance of the 2D PIO filtering algorithm [20], [27]. Point spread functions (PSFs) were simulated for illustrating the grating-lobe suppression using the proposed algorithm; cyst phantoms were simulated for showing the improved contrast in a speckle-generating scenario [20]. Various experiments have been further investigated using Ultrasonix RP system [28] with L14-5/38 linear array probe imaging the General Purpose Multi-Tissue Ultrasound Phantom (CIRS Model 040) [29], confirming the contrast improvement observed from the simulation results [27]. In addition to the contrast im-

This work was supported by NIH Grants EB 008191 and EB 006893 from NIBIB.

Yayun Wan is with the Department of Electrical and Computer Engineering, University of Minnesota, Minneapolis, USA. wanx0028@umn.edu

Emad S. Ebbini is with the Faculty of the Department of Electrical and Computer Engineering, University of Minnesota, Minneapolis, USA. ebbin001@umn.edu

provement, both experimental and simulation results demonstrated a well-behaved regularization process with properties changing gradually with increasing values of β. In particular, the resolutions, MGR (mainlobe-to-gratinglobe energy) and contrast ratio increase approximately as a smooth sigmoid function with respect to $\log(\beta)$. This not only proved the guaranteed robustness of the proposed pseudoinverse filtering algorithm, the sigmoid curved could also be used as a predictor of the imaging performance such as ranges of resolutions, contrast ratio predicted from MGR. Furthermore, This feature of the algorithm provides the convenience for the user to freely choose the value of β for achieving the desired levels of performance which can be implemented in much the same way as the TGC is implemented on current scanners. Another important characteristic of the algorithm is that it is intrinsically independent on the frequency of the array transducer, so it can also be used for lower-frequency arrays ($\leq$ 20 MHz) as well as high-frequency ones.

A spatial-temporal domain implementation of this filter has been proposed for the real-time implementation of this algorithm [27]. The 2D PIO filter was derived as a regularized pseudoinverse filtering operation in k-space preceded and followed by the 2D FFT operations [30]. The 2D regularized imaging operator was applied to the full frame data in k-space using computationally-efficient 2D FFT. The FFT size is at least the size of the full frame data plus the size of the frame system response in order to avoid aliasing. The observation of limited region of support for the filter in spatial-temporal domain makes it possible to operate the filter on a limited number of A-lines instead of the full frame data as in the case of filtering in k-space. This will be helpful for reducing the tissue motion sensitivity. Furthermore, while the FFT can be used for efficient computation of the filtering operation, spatial-domain may be more computationally efficient for finite-support filters, especially in real-time implementation with specialized hardware.

In this paper, we will demonstrate the *in vivo* verification of the imaging performance of the 2D PIO filtering algorithm. Experimental data on human carotid artery will be presented for illustrating the contrast restoration by using the proposed algorithm. Regularization process will be similarly tested for controlled imaging performance and robustness.

II. The 2D PIO Filtering Algorithm

The 2D PIO filtering algorithm was derived from the system model [21] on a Cartesian grid as illustrated in Figure 1. The system model has been generalized for frame acquisition from the original A-line acquisition system model [20].

Omitting the derivation details [20], the 2D PIO filtering algorithm can be summarized into three steps:

1) 2D discrete Fourier transformation (DFT) of the received frame of echo data $\{\mathbf{f}_m\}_{m=0}^{M-1}$ illustrated in Figure 1:

$$f_{K(k,n)} = \sum_{m=0}^{M-1}\sum_{l=0}^{N-1} \mathbf{f}_m(l) W_N^{nl} W_M^{mk}, \qquad (1)$$

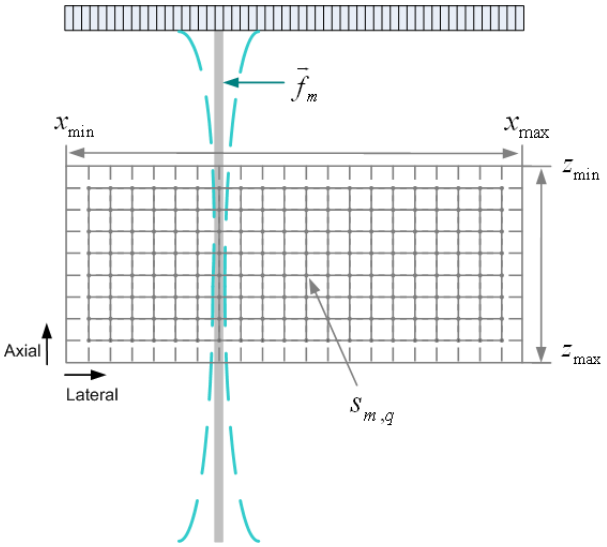

Fig. 1. A 1D linear array system model where the scattering is assumed to result from scatterers with random amplitudes on the Cartesian grid.

where, $W_N = e^{-j\frac{2\pi}{N}}$, $W_M = e^{-j\frac{2\pi}{M}}$, $\mathbf{f}_m(l)$ is the l_{th} sample in m_{th} A-line and $f_{K(k,n)}$ is the computed k-space representation (2D DFT coefficient) of the frame data.

2) 2D pseudoinverse filtering in k-space which is simply the multiplication between the k-space representation of the frame data $f_{K(k,n)}$ and the filter coefficients $d_{k,n}^{\dagger}$:

$$s_{Kk,n} = d_{k,n}^{\dagger} \cdot f_{K(k,n)}, \qquad (2)$$

where, the filter coefficients $d_{k,n}^{\dagger}$ is obtained by the regularization of $d_{k,n}$:

$$d_{k,n}^{\dagger} = \frac{d_{k,n}^{*}}{|d_{k,n}|^2 + \beta}, \qquad (3)$$

where β is a regularization parameter and $d_{k,n}$ is the k-space representation (2D DFT coefficient) of the 2D system impulse response. And the 2D impulse response can be obtained by a simulated model for forward propagation [20].

3) 2D inverse discrete Fourier transformation (IDFT) of the filtered results $s_{Kk,n}$ for obtaining the estimated scatterer distribution $\hat{s}_{m,q}$:

$$\hat{s}_{m,q} = \frac{1}{MN}\sum_{k=0}^{M-1}\sum_{q=0}^{N-1} s_{K(k,n)} W_N^{-nq} W_M^{-mk}, \qquad (4)$$

so completing the image reconstruction.

The filtering performance of the proposed algorithm can be adjusted by the choice of the regularization parameter β. We can sweep the value of β from small to large while the filter characteristics correspondingly change from inverse filtering (emphasizing resolution) to matched filtering (emphasizing SNR) with intermediate values being potential good compromises of the overall imaging performance.

III. Results and Discussion

In this section, we present experimental results from imaging human carotid artery *in vivo*. The carotid arteries are located on each side of the neck and carry blood from the heart to the brain. Ultrasound imaging on carotid arteries can be used for detecting the blockage or narrowing of the carotid arteries (conditions that substantially increase the risk of stroke), locating a hematoma, detecting dissection of the carotid artery or verifying the position of a metal stent placed to maintain carotid blood flow.

We used the Ultrasonix RP system [28] with L14-5/38 linear array probe. A simulated model for forward propagation was constructed based on the L14-5/38 linear array probe profile with the speed of sound set to be 1540 m/s as in soft tissue. The 2D filter coefficients were computed from the model using the 2D PIO filtering algorithm. An illustration of the 2D pseudoinverse filter representation is shown in Figure 2 with the regularization parameter set to be 1.

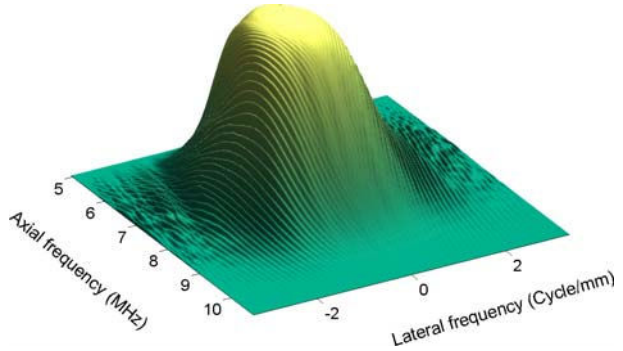

Fig. 2. The frequency response of the 2D PIO filter in k-space, applied to the carotid artery data with the regularization parameter β=1.

As shown in Figure 3, the center of the right carotid artery is at the depth of about 15 mm and its diameter is 6.5 mm. The probe was tilled slightly to reduce specular reflections from the artery walls. This may result in more clutter such as grating-lobe artifact from the tissue within the artery. The 50 dB grayscale images of the carotid artery before and after applying the 2D PIO filtering algorithm are shown in Figure 3 and Figure 4, respectively, both with a size of 27.4 mm $\times$ 38 mm. By comparing the PIO-filtered image with the unfiltered image, one can see a discernible difference in echogenicity from within the carotid. In addition, the speckle in tissue regions is generally well-behaved in the filtered image compared with the unfiltered one.

The contrast ratio (CR) was measured as 15.2 dB and 19 dB for the images in Figure 3 and Figure 4, respectively. In addition, the speckle correlation cell sizes [31] were measured as 286.6 μm and 284 μm in axial direction and 494.5 μm and 782.3 μm in lateral direction, respectively. Finally, the CR measurements from the *in vivo* results have a smooth changing pattern with respect to $\log_{10}\beta$. Specifically, it has an approximate sigmoidal behavior as shown in Figure 5, demonstrating a well-behaved regularization process which is one of the key reasons of the guaranteed robustness. This suggests that the user will be able to directly determine the level of regularization for achieving the desired levels of performance. This can be implemented in much the same way as the TGC is implemented on current scanners. All of these *in vivo* results are consistent with our previously reported results from computer simulations [20] as well as imaging of quality assurance phantoms [27], again verifying the imaging performance of the 2D PIO filtering algorithm such as contrast restoration.

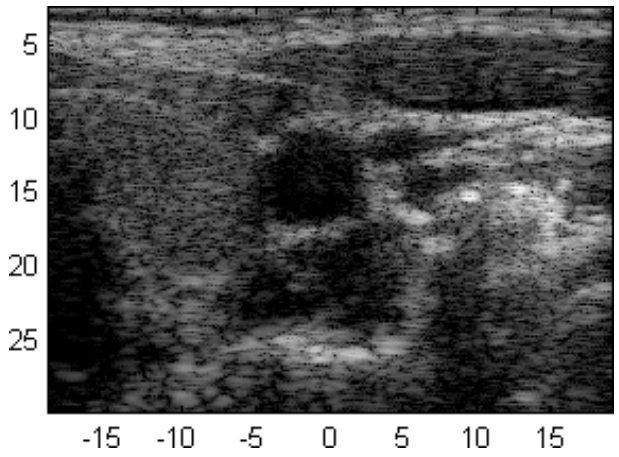

Fig. 3. The grayscale image (50 dB) of the right carotid artery, the vertical coordinate is axial direction, the horizontal coordinate is lateral direction and both are in mm.

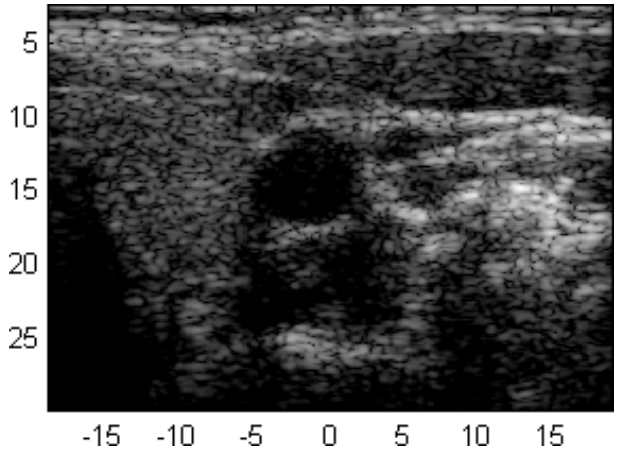

Fig. 4. The grayscale image (50 dB) of the right carotid artery, filtered by the 2D PIO filter, the vertical coordinate is axial direction, the horizontal coordinate is lateral direction and both are in mm.

IV. Conclusions

We presented a two-dimensional post-beamforming pseudoinverse filtering algorithm for restoration of contrast resolution in pulse-echo ultrasonic imaging systems using coarsely-sampled apertures. The performance of the filter was verified using images of human carotid artery *in vivo*. The results agreed with early simulation results and experimental results on quality-assurance phantoms. Specifically,

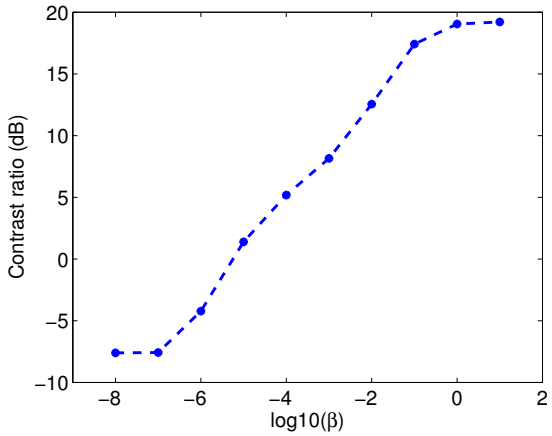

Fig. 5. Contrast ratio of results filtered by 2D PIO filter with sweeping regularization parameter β.

the *in vivo* results demonstrated similar contrast restoration and the well-behaved regularization process. Therefore, the 2D post-beamforming PIO approach described in this paper offers the promise of realizing the benefits of high-resolution ultrasonic imaging using coarsely sampled apertures.

V. ACKNOWLEDGMENTS

The authors would like to thank the Supercomputing Institute for Digital Simulation and Advanced Computation at University of Minnesota for their support of computational resources.

REFERENCES

[1] G. B. E. Jemec, M. Gniadecka, and J. Ulrich, "Ultrasound in dermatology. part I. high frequency ultrasound," *Eur. J. Dermatol.*, vol. 10, no. 6, pp. 492–497, Sep. 2000.

[2] F. S. Foster, C. J. Pavlin, K. A. Harasiewicz, D. A. Christopher, and D. H. Turnbull, "Advances in ultrasound biomicroscopy," *Ultrasound in Med. & Biol.*, vol. 26, no. 1, pp. 1–27, Jan. 2000.

[3] D. Liu and E. S. Ebbini, "Viscoelastic tissue property measurement using high frequency ultrasound," in *IEEE Int. Symp. on Biomed. Imag.*, Apr. 2007, pp. 892–895.

[4] D. T. Yeh, O. Oralkan, I. O. Wygant, M. O'Donnell, and B. T. Khuri-Yakub, "3D ultrasound imaging using a forward-looking CMUT ring array for intravascular/intracardiac applications," *IEEE Trans. Ultrason., Ferroelect., Freq. Contr.*, vol. 53, no. 6, pp. 1202–1211, Jun. 2006.

[5] S. E. Nissen and P. Yock, "Intravascular ultrasound: novel pathophysiological insights and current clinical applications," *Circulation*, vol. 103, pp. 604–616, 2001.

[6] M. R. Neidert and R. Tranquillo, "Tissue engineered valves with commissural alignment," *Tissue Eng.*, vol. 12, no. 4, pp. 891–903, Apr. 2006.

[7] J. B. Liu and B. B. Goldberg, "Endoluminal vascular and nonvascular sonography: past, present, and future," *AJR Am. J. Roentgenol.*, vol. 165, no. 4, pp. 765–774, Oct. 1995.

[8] H. K. W. Kim, P. S. Babyn, K. A. Harasiewicz, K. P. H. Pritzker, and F. S. Foster, "High resolution imaging of articular cartilage using ultrasound biomicroscopy," *J. Orthopaed Res.*, vol. 13, pp. 963–970, 1995.

[9] D. H. Turnbull, J. A. Ramsay, G. S. Shivji, T. S. Bloomfield, L. From, D. N. Sauder, and F. S. Foster, "Ultrasound backscatter microscope analysis of mouse melanoma progression," *Ultrasound in Med. & Biol.*, vol. 22, no. 7, pp. 845–853, 1996.

[10] M. Lukacs, J. Yin, G. Pang, R. C. Garcia, E. Cherin, R. Williams, J. Mehi, and F. S. Foster, "Performance and characterization of new micromachined high-frequency linear arrays," *IEEE Trans. Ultrason., Ferroelect., Freq. Contr.*, vol. 53, no. 10, pp. 1719–1729, Oct. 2006.

[11] J. A. Brown, F. S. Foster, A. Needles, E. Cherin, and G. R. Lockwood, "Fabrication and performance of a 40-mhz linear array based on a 1-3 composite with geometric elevation focusing," *IEEE Trans. Ultrason., Ferroelect., Freq. Contr.*, vol. 54, no. 9, pp. 1888–1894, Sep. 2007.

[12] A. Nguyen-Dinh, L. Ratsimandresey, P. Mauchamp, R. Dufait, A. Flesch, and M. Lethiecq, "High frequency piezo-composite transducer array designed for ultrasound scanning applications," in *IEEE Ultrason. Symp.*, vol. 2, 1996, pp. 943–947.

[13] T. A. Ritter, K. K. Shung, J. Cannata, and T. R. Shrout, "High frequency ultrasound arrays for medical imaging," in *IEEE Ultrason. Symp.*, vol. 2, 2000, pp. 1261–1264.

[14] R. Liu, K. A. Harasiewicz, and F. S. Foster, "Interdigital pair bonding for high frequency (20-50 MHz) ultrasonic composite transducers," *IEEE Trans. Ultrason., Ferroelect., Freq. Contr.*, vol. 48, no. 1, pp. 299–306, Jan. 2001.

[15] E. Lacaze, S. Michau, and P. Mauchamp, "20 MHz ultrasound array for medical imaging: from design to image evaluation," in *IEEE Ultrason. Symp.*, vol. 2, 2001, pp. 1139–1142.

[16] T. A. Ritter, T. R. Shrout, R. Tutwiler, and K. K. Shung, "A 30 MHz piezo-composite ultrasound array for medical imaging applications," *IEEE Trans. Ultrason., Ferroelect., Freq. Contr.*, vol. 49, no. 2, pp. 217–230, Feb. 2002.

[17] W. Hackenberger, S. Kwon, P. Rehrig, K. Snook, and S. Rhee, "2-2 PZT-polymer composites for high frequency (>20 MHz) ultrasound transducers," in *IEEE Ultrason. Symp.*, vol. 2, 2002, pp. 1253–1256.

[18] S. Michau, P. Mauchamp, and R. Dufait, "Piezocomposite 30MHz linear array for medical imaging: design challenges and performances evaluation of a 128 elements array," in *IEEE Ultrason. Symp.*, vol. 2, 2004, pp. 898–901.

[19] D. T. Yeh, O. Oralkan, A. S. Ergun, X. Zhuang, I. O. Wygant, and B. T. Khuri-Yakub, "High-frequency CMUT arrays for high-resolution medical imaging," in *Proc. SPIE Med. Imag.*, vol. 5750, Apr. 2005, pp. 87–98.

[20] Y. Wan and E. S. Ebbini, "A post-beamforming 2d pseudoinverse filter for coarsely sampled ultrasound arrays," *IEEE Trans. Ultrason., Ferroelect., Freq. Contr.*, 2009, in press.

[21] J. Shen and E. S. Ebbini, "Filter-based coded-excitation system for high-speed ultrasonic imaging," *IEEE Trans. Med. Imag.*, vol. 17, no. 6, pp. 923–934, 1998.

[22] R. Y. Chiao and X. Hao, "Coded excitation for diagnostic ultrasound: A system developer's perspective," *IEEE Trans. Ultrason., Ferroelect., Freq. Contr.*, vol. 52, no. 2, pp. 160–170, Feb. 2005.

[23] B. Haider, P. A. Lewin, and K. E. Thomenius, "Pulse elongation and deconvolution filtering for medical ultrasonic imaging," *IEEE Trans. Ultrason., Ferroelect., Freq. Contr.*, vol. 45, no. 1, pp. 98–113, Jan. 1998.

[24] M. Vogt and H. Ermert, "In vivo ultrasound biomicroscopy of skin: Spectral system characteristics and inverse filtering optimization," *IEEE Trans. Ultrason., Ferroelect., Freq. Contr.*, vol. 54, no. 8, pp. 1551–1559, Aug. 2007.

[25] T. Misaridis and J. A. Jensen, "Use of modulated excitation signals in medical ultrasound. part I: basic concepts and expected benefits," *IEEE Trans. Ultrason., Ferroelect., Freq. Contr.*, vol. 52, no. 2, pp. 177–191, Feb. 2005.

[26] J. Shen and E. S. Ebbini, "A new coded-excitation ultrasound imaging system – part I: basic principles," *IEEE Trans. Ultrason., Ferroelect., Freq. Contr.*, vol. 43, no. 1, pp. 131–140, Jan. 1996.

[27] Y. Wan and E. S. Ebbini, "2d filter design for the reduction of beamforming artifacts in coarsely-sampled imaging apertures," *IEEE Ultrason. Symp.*, 2008, in press.

[28] "Ultrasonix RP system." [Online]. Available: http://www.ultrasonix.com/systems/sonix-rp.php

[29] "CIRS Model 040." [Online]. Available: http://www.cirsinc.com/040_overv.html

[30] Y. Wan and E. S. Ebbini, "A post-beamforming 2d pseudoinverse filter for coarsely sampled ultrasound arrays," in *IEEE Ultrason. Symp.*, Oct. 2007, pp. 21–24.

[31] R. F. Wagner, M. F. Insana, and S. W. Smith, "Fundamental correlation lengths of coherent speckle in medical ultrasonic images," *IEEE Trans. Ultrason., Ferroelect., Freq. Contr.*, vol. 35, no. 1, pp. 34–44, 1988.